Journal of Alloys and Compounds 509 (2011) 3177–3182

Contents lists available at ScienceDirect

Journal of Alloys and Compounds

journal homepage: www.elsevier.com/locate/jallcom

# Boron doped nanostructure ZnO films onto ITO substrate

Mujdat Caglar[a,*], Saliha Ilican[a], Yasemin Caglar[a], Fahrettin Yakuphanoglu[b]

[a] Anadolu University, Department of Physics, 26470 Eskisehir, Turkey
[b] Firat University, Department of Metallurgical and Materials Engineering, Elazig, Turkey

ARTICLE INFO

*Article history:*
Received 13 November 2010
Received in revised form 6 December 2010
Accepted 7 December 2010
Available online 14 December 2010

*Keywords:*
B doped ZnO
Sol–gel
Nanostructure film
Activation energy
Space charge limited current

ABSTRACT

Undoped and boron (B) doped nanostructure ZnO films were prepared by sol–gel method using spin coating technique. The effects of B content on the crystallinity and morphological properties of ZnO films were analyzed by X-ray diffractometer, field emisison scanning electron microscopy (FESEM) and atomic force microscopy (AFM). X-ray diffraction (XRD) patterns confirm the hexagonal wurtzite type polycrystalline structure of the films and the incorporation of boron leads to substantial changes in the structural characteristics of ZnO films. The FESEM and AFM measurements indicated that the surface morphology of the films was affected from the boron incorporation. The absorption spectra revealed that B doped ZnO films had a optical band gap exhibiting directly optical transtions and optical band gap of the films decreased with the increase in temperature. The electrical conductivity dependence of temperature of the 5% boron doped nanostructure ZnO film revealed that the conduction mechanism of the film was an extrinsic conductivity mechanism with shallow and deep trap levels. At higher electric fields, the conductivity mechanism of the film was controlled by space charge limited current mechanism.



## 1. Introduction

Transparent conducting zinc oxide (ZnO) films have been extensively studied in recent years because they can be made to have high electrical conductivity, high infrared reflectance, and high visible transmittance. So, these films have numerous industrial applications, such as energy efficient windows, solar cells, liquid crystal displays, and other optoelectronic devices. ZnO films are prepared by various techniques such as chemical vapor deposition [1], spray pyrolysis [2,3], thermal evaporation [4], r.f. magnetron sputtering [5], and sol–gel method [6,7]. Among these methods, sol–gel process is an attractive technique for obtaining film because it has advantages of easy control of the film composition, homogeneity, large area coating capability and easy fabrication of large-area films with low cost. Moreover, this process allows doping of various materials, which makes it possible to fabricate thin, transparent and multicomponent oxide films.

ZnO is a II–VI compound semiconductor with a wurtzite structure and it has a wide direct band gap of 3.37 eV at room temperature. ZnO is naturally an n-type semiconductor due to deviation from stoichiometry. The free charge carriers mainly arise from the shallow donor levels associated with oxygen vacancies and interstitial zinc atoms. Hence, the increase in conductivity of ZnO can be obtained by controlling these native defects. Higher conductivity n-type ZnO films can be easily obtained by doping group III elements such as B, Al, In and Ga in the substitution of zinc atoms [8–11] or group VII elements, for example, F, in the substitution of oxygen atoms [12].

It is well-known that the optical band gap of semiconductors changes with temperature. For example, the optical band gap of bulk ZnO is 3.436 eV at 4.2 K [13] and 3.37 eV at 300 K, the band gap shows a linear relation with temperature. Also, it is important and necessary to have knowledge about it, because in many of the potential applications of semiconductor, the working temperature is either elevated or reduced.

Although there is not too much works about boron doped ZnO films [14–18], there is only a few study related to boron doped ZnO deposited by sol–gel method in among of them. Tahar and Tahar [19] used sol–gel dip coating method and investigated the electrical and optical properties of multilayer transparent conducting boron doped ZnO films according to various deposition parameters. Houng et al. [20] reported the effect of pH of precursor sol on the crystallization, microstructure, electrical and optical properties of sol–gel derived boron doped ZnO oxide transparent conducting thin films. In this paper, we both report the effects of the boron doping on the physical properties of ZnO films and a detailed study of the temperature dependence (in the temperature region 80–460 K) of optical band gap for undoped and boron doped ZnO films.

* Corresponding author. Tel.: +90 222 3350580; fax: +90 222 3204910.
*E-mail addresses:* mcaglar@anadolu.edu.tr, mcaglar@semiconductorslab.com (M. Caglar).

0925-8388/$ – see front matter © 2010 Elsevier B.V. All rights reserved.
doi:10.1016/j.jallcom.2010.12.038

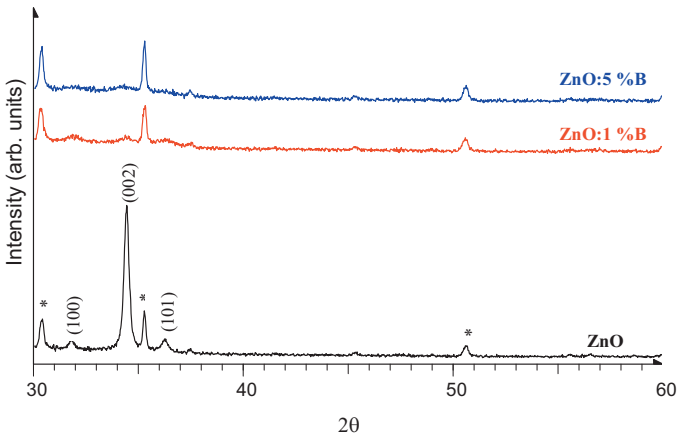


**Fig. 1.** X-ray diffraction spectra of the undoped and B doped nanostructure ZnO films (*: ITO substrate).

**Table 1**
The optical band gap values of the undoped and B doped ZnO films.

| ZnO | | ZnO:1% B | | ZnO:5% B | |
|---|---|---|---|---|---|
| $T$ (K) | $E_g$ (eV) | $T$ (K) | $E_g$ (eV) | $T$ (K) | $E_g$ (eV) |
| 80 | 3.404 | 80 | 3.227 | 80 | 3.224 |
| 100 | 3.397 | 100 | 3.224 | 100 | 3.223 |
| 120 | 3.394 | 120 | 3.225 | 120 | 3.214 |
| 140 | 3.386 | 140 | 3.223 | 140 | 3.218 |
| 165 | 3.387 | 160 | 3.221 | 160 | 3.216 |
| 200 | 3.373 | 200 | 3.211 | 200 | 3.209 |
| 240 | 3.366 | 240 | 3.207 | 240 | 3.196 |
| 280 | 3.355 | 250 | 3.202 | 250 | 3.192 |
| 300 | 3.348 | 280 | 3.193 | 280 | 3.181 |
| 320 | 3.346 | 300 | 3.191 | 300 | 3.175 |
| 340 | 3.334 | 310 | 3.187 | 320 | 3.163 |
| 360 | 3.318 | 320 | 3.189 | 340 | 3.127 |
| 380 | 3.311 | 340 | 3.183 | 360 | 3.116 |
| 400 | 3.303 | 380 | 3.176 | 380 | 3.112 |
| 420 | 3.294 | 400 | 3.163 | 400 | 3.110 |
| 440 | 3.293 | 420 | 3.150 | 420 | 3.098 |
| 460 | 3.287 | 440 | 3.146 | 440 | 3.095 |
| | | 460 | 3.134 | 460 | 3.096 |

## 2. Experimental details

### 2.1. Deposition of the undoped and boron doped nanostructure ZnO films

Undoped and boron doped nanostructure ZnO films were prepared by sol–gel method onto indium tin oxide (ITO) coated glass substrates. Zinc acetate dihydrate [$Zn(CH_3COO)_2{\cdot}2H_2O$] (ZnAc) was used as a starting material. 2-Methoxethanol ($C_3H_8O_2$) and ethanolamine [$C_2H_7NO$] (MEA) were used as a solvent and stabilizer. The dopant source of boron came from trimethyl borate [$(B(OCH_3)_3)$] (TMB). The molar ratios of MEA to ZnAc and TMB were maintained at 1:1. The B/Zn nominal ratio was 1% and 5%. The solution was stirred for 2 h at 60 °C to yield a clear homogeneous and transparent solution using a magnetic stirrer. The ITO substrates firstly were cleaned by detergent, and then in methanol and acetone using an ultrasonic cleaner. The coating solution was dropped into an ITO substrate, which was rotated at 3000 rpm for 30 s using spin coater. After the spin coating, the film was dried at

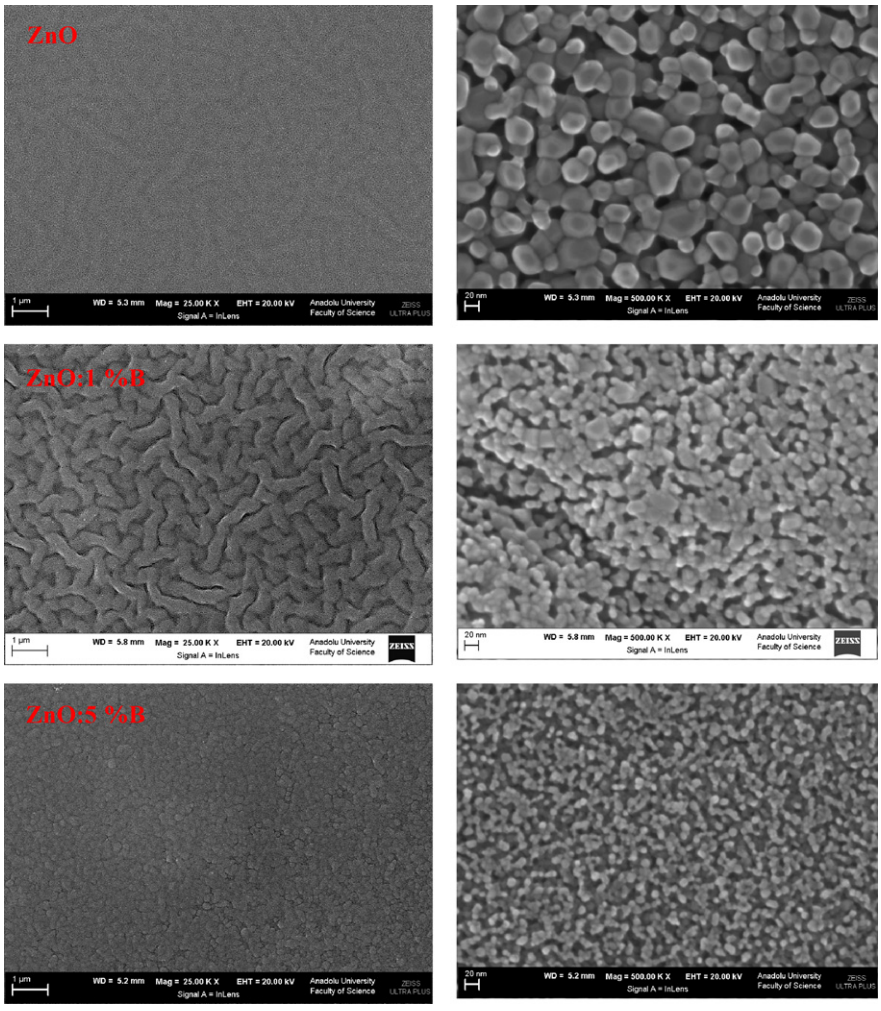


**Fig. 2.** FESEM images of the undoped and B doped nanostructure ZnO films.

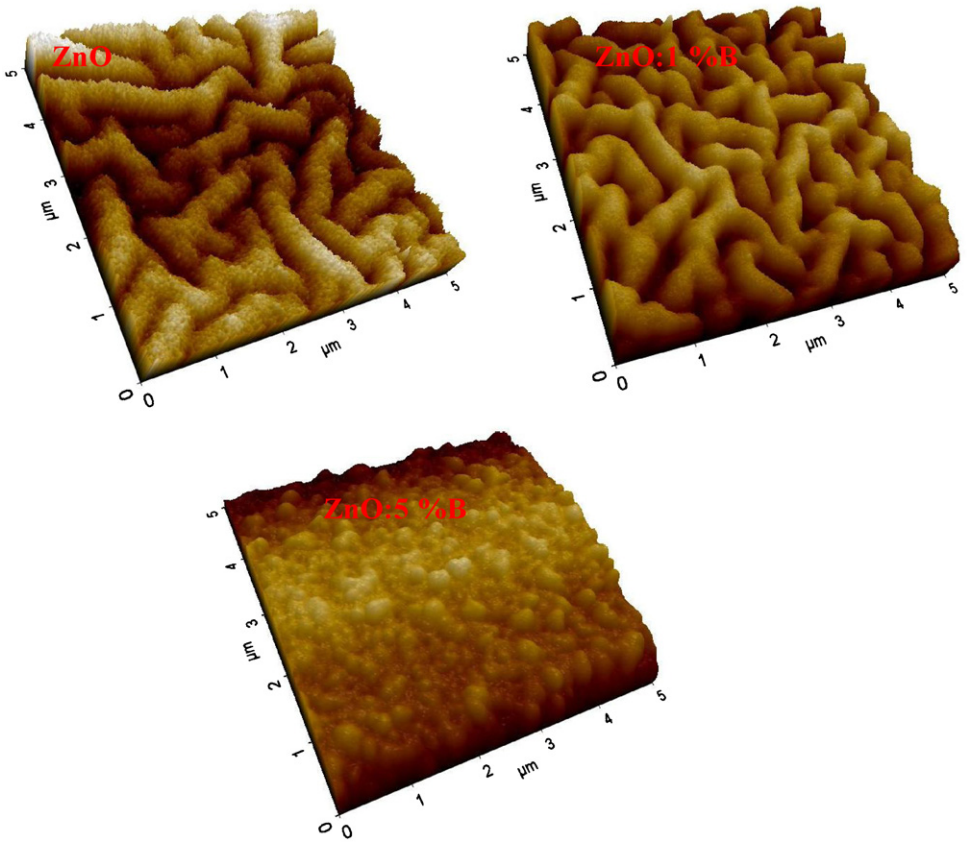


**Fig. 3.** AFM images of the undoped and B doped nanostructure ZnO films.

300 °C for 10 min in a furnace to evaporate the solvent and to remove organic residuals. Ten cycles of coating and heating were performed. Finally the samples were annealed at 500 °C an hour in air. This coating process was performed for all the films. The thickness of the films were determined with Mettler Toledo MX5 microbalance using weighing method and found to be 546, 487 and 640 nm for ZnO, 1% B doped ZnO (ZnO:1% B) and 5% B doped ZnO (ZnO:5% B), respectively.

### 2.2. Characterization of the undoped and boron doped nanostructure ZnO films

XRD experiments were performed in air with a laboratory X-ray powder diffractometer at room temperature. The films were mounted on rotating sample holders. A sealed X-ray tube operated at 40 kV and 40 mA with Cu Kα radiation was used. All measurements were performed in reflection geometry as coupled $\theta$–$2\theta$ scans ($30^\circ \leq 2\theta \leq 60^\circ$). Surface morphology was studied using a ZEISS Ultraplus model field emission scanning electron microscopy (FESEM) and PARK System XE100 atomic force microscopy (AFM). The temperature-dependent absorption measurements of the films were carried out using Ocean Optics Spectrophotometer with in Janis VPF 475 cryostat in the range of 77–500 K. The temperature of the films was controlled using a Lakeshore 331S temperature controller and it was measured with an accuracy of 0.01 K. The temperature-dependent electrical measurements of the films were performed in a furnace and in the temperature range 300–460 K using Keithley 4200SCS Semiconductor Characterization System.

## 3. Results and discussion

### 3.1. Structural properties of the undoped and boron doped nanostructure ZnO films

The XRD patterns of ZnO, ZnO:1% B and ZnO:5% B nanostructure films are shown in Fig. 1. The ZnO film was found to be polycrystalline with a (0 0 2) preferred orientation. Secondary peaks detected were (1 0 0) and (1 0 1). It was further found that the incorporation of boron resulted in decrease in the intensity of the (0 0 2) peak. According to XRD results, it is shown that the crystallinity of the ZnO film deteriorated with boron incorporation.

The same tendency was also observed by Kim et al. [14]. It was seen that boron doping resulted in an interstitial inclusion of dopant atoms, which resulted in a deterioration of the film structure. This indicates that higher content of boron leads to a deterioration of the crystal structure by distorting the ZnO lattice. Some lattice defects and distortion of the crystal lattice are induced because of differently sized atoms substitute in the ZnO lattice.

The surface morphological features of the films were analyzed using FESEM. Fig. 2 shows high resolution FESEM images of the films. The incorporation of boron in ZnO film significantly alters both the surface morphology and the crystallite size. Undoped ZnO crystallite size is approximately 20–30 nm, but crystallite size of boron doped ZnO is quite smaller than the undoped one. Also, the grain boundaries clearly disappeared due to the incorporation of boron. While the hexagonal shape particles can be clearly seen in the FESEM image of ZnO, in the images of doped ZnO, the particles size decreases and the particle shape is round.

AFM images were assessed over a $5 \times 5\,\mu m$ area by non-contact mode. AFM (3D) studies of the surface morphology are shown in Fig. 3 for undoped and B doped ZnO films. A wrinkle network is seen in ZnO and ZnO:1% B films. Especially in the ZnO film image, the crystallite size can be noticeable from the AFM image, but not seen in the other doped samples. This decrease in crystallite size depending on the boron doping is also seen from the FESEM images. Also the wrinkle network disappeared in the ZnO:5% B film. Finally the boron incorporation to ZnO film significantly affects the surface morphology of the film.

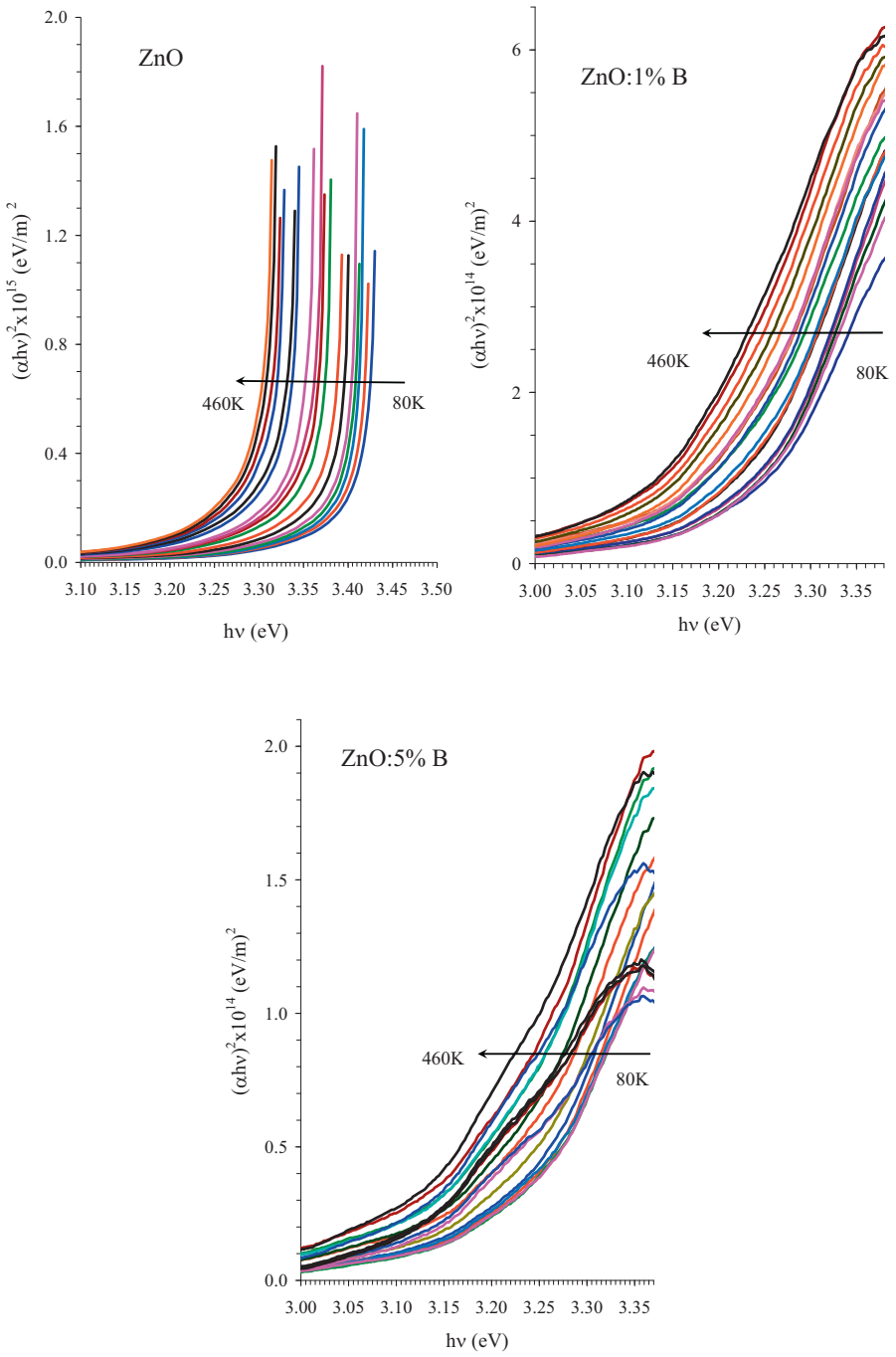


**Fig. 4.** Plots of $(\alpha h\upsilon)^2$ vs. photon energy of the undoped and B doped nanostructure ZnO films at various temperatures.

### 3.2. Temperature dependence of the optical band gap of the undoped and boron doped nanostructure ZnO films

Analysis of optical absorption spectra is one of the most productive tools for determining optical band gap of the films. From these spectral data, the absorption coefficient, $\alpha$, was calculated using the relationship [21],

$$\alpha h\nu = B(h\nu - E_g)^{1/2} \quad (1)$$

where $\alpha$ is absorption coefficient, $B$ is an energy-independent constant and $E_g$ is the optical band gap with allowed direct transitions. The optical band gap of the ZnO film has a direct optical transition.

For the undoped and boron doped nanostructure ZnO films, the absorption spectra were recorded at different temperatures varying from 80 to 460 K. The $E_g$ values could be obtained by the extrapolating method using the $(\alpha h\nu)^2$ vs. $h\nu$ plot. Fig. 4 shows plots of $(\alpha h\nu)^2$ vs. $h\nu$ for the undoped and boron doped nanostructure ZnO films. The $E_g$ values for the films are given in Table 1. As seen from this Table, these values decrease with increasing temperature. Namely, it shifts from 3.404 eV to 3.287 eV for the ZnO film, from 3.227 eV to 3.134 eV for the ZnO:1% B film and from 3.224 eV to 3.096 eV for the ZnO:5% B film as temperature varies from 80 to 460 K. The optical band gaps of the ZnO film decrease with B incorporation at the various temperatures. A red shift in the absorption edge of ZnO film with B incorporation is also observed.

The temperature dependence of the optical band gap of nanostructure ZnO films is presented in Fig. 5. This figure was fitted by some functions. ZnO film indicates a linear relationship between

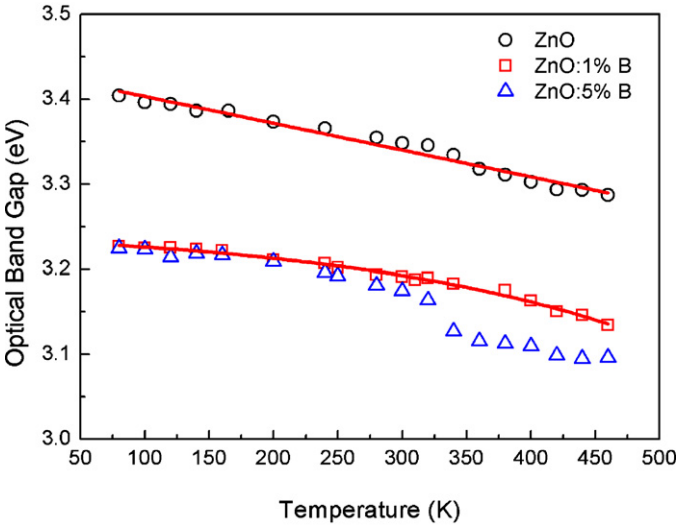


**Fig. 5.** Temperature dependence of the optical band gap of the undoped and B doped nanostructure ZnO films.

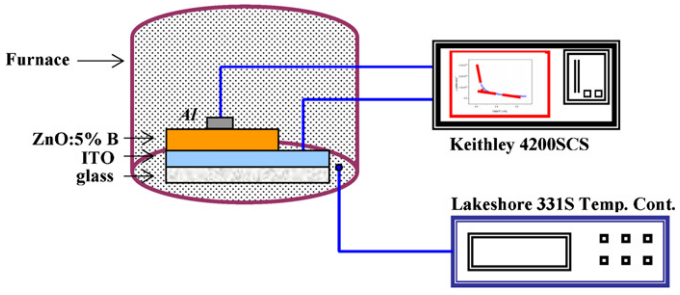


**Fig. 6.** The experimental configuration used for electrical conductivity measurement.

optical and temperature and thus, the temperature dependence of the optical energy band gap of ZnO film is well fitted by the following formula [22]

$$E_g(T) = E_g(0) + \beta T \quad (2)$$

where $E_g(0)$ is the energy at 0 K and $\beta$ is the rate of change of the band gap with temperature. Fig. 5 was fitted and the obtained the best fitting parameters of $E_g(0)$ and $\beta$ were found to be 3.435 eV and $-3.15 \times 10^{-4}$ eV K$^{-1}$, respectively. The negative $\beta$ value shows that

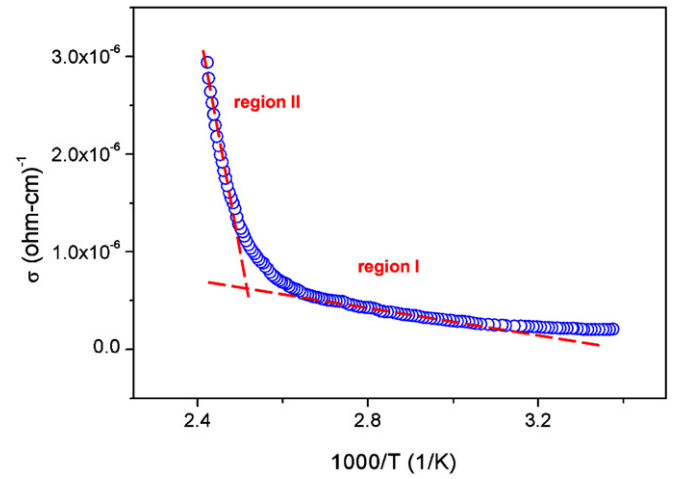


**Fig. 7.** Plot of $\sigma$ vs. 1000/$T$ of the ZnO:5% B film.

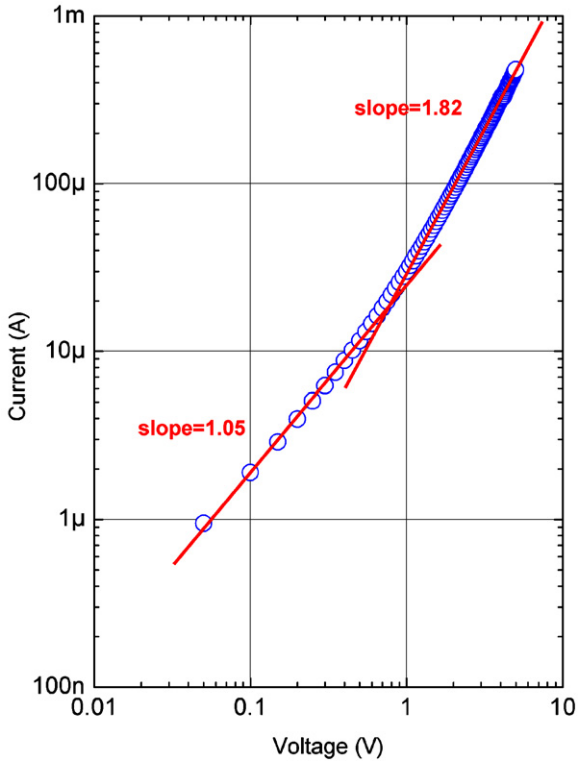


**Fig. 8.** The plot of current–voltage of the ZnO:5% B film at room temperature.

the valence band goes up towards the conduction band [23]. The variation of optical band gap with temperature for ZnO:1% B film exhibits a exponential variation by defined function. The variation of optical band gap with temperature for ZnO:1% B film was defined by the following function,

$$E_g(T) = E_g(0) + \frac{A_1 \exp(T - T_0)}{t} \quad (3)$$

where $E_g(0)$, $A_1$, $T_0$ and $t$ are fitting parameters and these parameters were found to be $E_g(0) = 3.249$ eV, $A_1 = -0.01676$ eV, $T_0 = 18.267$ K and $t = 230.432$ K, respectively. On the other hand, the change in optical band gap of ZnO:5% B film does not obey any fit function. The decrease in the optical band gap of the ZnO films is due to changing interatomic distances of undoped and B doped ZnO samples. This change may be attributed to a shift in the relative positions of the valance and conduction bands due to the temperature dependence of the dilation of the lattice and the temperature-dependent electron–lattice interaction [24]. Electron–phonon interactions depending on temperature cause a renormalization of the band energies and in turn, the optical band decreases with the temperature.

### 3.3. Electrical properties of ZnO:5% B film

The electrical conductivity of the ZnO:5% B film was measured in dark and in a furnace, in the range of temperature from 300 to 460 K. The experimental configuration used for electrical conductivity measurement is given in Fig. 6. Fig. 7 shows plot of $\sigma$ vs. 1000/$T$ for the film. The temperature dependence of conductivity shows different two regions. These regions arise from different conduction processes. The conductivity increases with increasing temperature. The ZnO:5% B film has the carrier electrons excited thermally from donor levels formed by the incorporation of boron atoms into the ZnO lattice. As the temperature is increased, more charge carriers overcome the activation energy barrier and participate in the electrical conduction. The temperature dependence of

the conductivity can be represented by the formula

$$\sigma = \sigma_0 \exp\left(-\frac{E}{kT}\right) \quad (4)$$

where and $\sigma_0$ is the pre-exponential factor, $T$ is absolute temperature, $k$ is Boltzmann constant and $E$ is the activation energy corresponding to the energy difference between donor level and conduction level. $E_I$ and $E_{II}$ activation energy values for I and II regions were respectively calculated from the linear portions of Fig. 7. The obtained $E_I$ and $E_{II}$ values are 0.160 eV and 0.850 eV, respectively. It is well known that the electrical conductivity of ZnO at room temperature is due to the oxygen vacancy and interstitial zinc atom, which act as donors. These defects introduce donor states in the forbidden band slightly below the conduction band and hence resulting in the conducting behavior of ZnO. This electrical conductivity can be controlled by the intrinsic defects generated during synthesis and by the presence of dopants. Therefore, $E_I$ activation energy corresponding to first conductivity region results from shallow donor levels and $E_{II}$ activation energy corresponding to second conductivity region results from deep donor levels can be associated with the Zn interstitials, oxygen vacancies, or boron which acts as donors in the ZnO lattice.

In order to analyze conduction mechanism of the ZnO:5% B film at higher electric fields, the current–voltages characteristics in double logarithmic scale of ZnO:5% B nanostructure film at room temperature are shown in Fig. 8. The forward bias log $I$–log $V$ curve is characterized by two distinct linear regions, indicating different conduction mechanisms. The $I$–$V$ curve exhibits ohmic conduction at low voltage where the logarithmic slope is about unity. In this region, the thermally generated carriers are predominant over the injected carriers. With the applied voltage increasing, the slopes of the $I$–$V$ curve changes from 1.05 to 1.82, indicating that a space charge-limited current (SCLC) mechanism is controlled by the presence of traps within the band gap of ZnO:5% B doped film.

## 4. Conclusions

Undoped and B doped nanostructure ZnO films were deposited by sol–gel method using spin coating technique. The structural, morphological, optical and electrical properties of these films were investigated. According to XRD results, it was shown that the crystallinity of the ZnO film deteriorated with boron incorporation. The incorporation of boron in ZnO film significantly altered both the surface morphology and the crystallite size. It was shown a wrinkle network in the ZnO film surface from both FESEM and AFM results. This network disappeared with increasing boron incorporation and it was observed that the surface was smoother with increasing B content. The optical absorptions of the ZnO film were carried out between 80 and 460 K temperatures. The parameters that describe the temperature variations of the optical band gap in the ZnO film were evaluated and discussed. The transport mechanisms in the ZnO:5% B film were investigated by analyzing the temperature dependent conductivity values. The activation energies of shallow and deep donor levels were obtained as 0.160 eV and 0.850 eV, respectively. From the forward bias $I$–$V$ measurements, the presence of traps was determined.

## Acknowledgements

This work was supported by the National Boron Research Institute (BOREN) (Grant No: BOREN-2009.Ç0226). Authors wish to thank Anadolu University Faculty of Science for FESEM measurements.

## References

[1] M.R. Wagner, T.P. Bartel, R. Kirste, A. Hoffmann, J. Sann, S. Lautenschlager, B.K. Meyer, C. Kisielowski, Phys. Rev. B 79 (2009) 035307.
[2] M. Caglar, S. Ilican, Y. Caglar, F. Yakuphanoglu, J. Mater. Sci.: Mater. Electron. 19 (2008) 704–708.
[3] S. Ilican, Y. Caglar, M. Caglar, F. Yakuphanoglu, Physica E 35 (2006) 131–138.
[4] L.B. Feng, A.H. Liu, M. Liu, Y.Y. Ma, J. Wei, B.Y. Man, J. Alloys Compd. 492 (2010) 427–432.
[5] Y.P. Liao, J.H. Zhang, S.X. Li, Z.S. Guo, J. Cao, W.Q. Zhu, X.F. Li, Phys. Status Solidi A: Appl. Mater. Sci. 207 (2010) 1850–1853.
[6] S. Ilican, M. Caglar, Y. Caglar, Appl. Surf. Sci. 256 (2010) 7204–7210.
[7] F. Yakuphanoglu, S. Ilican, M. Caglar, Y. Caglar, Superlattices Microstruct. 47 (2010) 732–743.
[8] X.D. Liu, E.Y. Jiang, Z.Q. Li, J. Appl. Phys. 102 (2007) 073708.
[9] Y. Caglar, S. Ilican, M. Caglar, F. Yakuphanoglu, Spectrochim. Acta A 67 (2007) 1113–1119.
[10] K.S. Shin, K.H. Lee, H.H. Lee, D. Choi, S.W. Kim, J. Phys. Chem. C 114 (2010) 15782–15785.
[11] S.H. Yang, S.Y. Hong, C.H. Tsai, Jpn. J. Appl. Phys. 49 (2010) 06GJ06.
[12] S. Ilican, Y. Caglar, M. Caglar, F. Yakuphanoglu, Appl. Surf. Sci. 255 (2008) 2353–2359.
[13] T. Yamamoto, Phys. Status Solidi A 193 (2002) 423–433.
[14] G. Kim, J. Bang, Y. Kim, S.K. Rout, S. IhlWoo, Appl. Phys. A 97 (2009) 821–828.
[15] X.L. Chen, B.H. Xu, J.M. Xue, Y. Zhao, C.C. Wei, J. Sun, Y. Wang, X.D. Zhang, X.H. Geng, Thin Solid Films 515 (2007) 3753–3759.
[16] S.Y. Myong, J. Steinhauser, R. Schluchter, S. Fay, E.V. Sauvain, A. Shah, C. Ballif, A. Rufenacht, Sol. Energy Mater. Sol. Cells 91 (2007) 1269–1274.
[17] B.N. Pawar, S.R. Jadkar, M.G. Takwale, J. Phys. Chem. Solids 66 (2005) 1779–1782.
[18] A.E. Rakhshani, J. Phys. D: Appl. Phys. 41 (2008) 015305.
[19] R.B.H. Tahar, N.B.H. Tahar, J. Mater. Sci. 40 (2005) 5285–5289.
[20] B. Houng, C.L. Huang, S.Y. Tsai, J. Cryst. Growth 307 (2007) 328–333.
[21] N.F. Mott, R.W. Gurney, Electronic Processes in Ionic Crystals, Oxford Univ. Press, London, 1940.
[22] X. Mathew, N.R. Mathews, P.J. Sebastian, Sol. Energy Mater. Sol. Cells 70 (2001) 277.
[23] F. Yakuphanoglu, M. Arslan, M. Küçükislamoğlu, M. Zengin, Sol. Energy 79 (2005) 96–100.
[24] B.S. Li, Y.C. Liu, Z.Z. Zhi, D.Z. Shen, Y.M. Lu, X.W. Zhang, X.W. Fan, J. Cryst. Growth 240 (2002) 497.